Exploring Cu-based spinel/delafossite couples for thermochemical energy storage at medium-high temperature

Xiaoyu Chen[a], Mitsuhiro Kubota[a*], Seiji Yamashita[b], Hideki Kita[a]

[a]Nagoya University, Graduate school of Engineering, Department of Chemical Systems Engineering, Nagoya 4648603, Japan

[b]Nagoya University, Graduate school of Engineering, Department of Materials Process Engineering, Nagoya 4648603, Japan

Abstract:

Cu-based spinel/delafossite couples with Mn and Fe as a second cation were synthesized using the Pechini method for medium-high temperature thermochemical energy storage. Physicochemical property of each sample was investigated. Only $CuMn_2O_4/CuMnO_2$ exhibited favorable redox behavior in the range of 500-1000 °C. Cu-based delafossite can re-oxidize at a lower temperature (~600 °C), which may be related to the existence of MO_6 octahedra structure. Through isothermal oxidation method, $CuMn_2O_4/CuMnO_2$ couple showed larger oxidation enthalpy of 258.32 ± 15.31 kJ/kg (1402.68 ± 83.13 kJ/L) than 190.35 ± 4.81 kJ/kg (1048.83 ± 26.50 kJ/L) of $CuFe_2O_4/CuFeO_2$ couple. $CuMn_2O_4$ was chosen for further cyclability test with 20 cycles, the depth of reduction increased gradually and stabilized at 4 % change in mass after 13 cycles.

Keywords: heat storage; TCES; medium-high temperature; Cu-based oxides; spinels; delafossites

1. Introduction

Compared with conventional sensible and latent thermal energy storage techniques, thermochemical energy storage (TCES) system has become a research hotspot in the field of thermal energy utilization recently, because of its larger energy storage density, wider range of operational temperature and unlimited transportation distance[1]. Redox-type TCES is one of the most important system because oxygen works as heat transfer fluid and reactant [Eq. (1)], meaning that it does not require a gaseous tank for the storage of product because oxygen can be easily extracted from air[2].

$$MO_{oxidation\ state} + \Delta H_r \rightleftharpoons MO_{reduction\ state} + O_2 \quad (1)$$

Currently, redox-type TCES technology is primarily applied for ultra-high temperature solar energy utilization[3,4]. However, other thermal energy storage fields, such as heat recycling of exhaust gas from the steel industry, and in-car heating of electric vehicles during the winter season, can be also benefited from mature TCES technology. For practical use, such applications cannot be operated under excessively high temperature, or high-temperature condition is not required. In particular, volume restrictions for heat storage equipment exist in electric vehicle design.

As redox-type TCES is a fledgling technology, most researchers focus on high-temperature (>1000 °C) heat storage for CSP (Concentrated solar power) purposes, meanwhile, the development of medium-high temperature (500-1000 °C) technology remains stagnant, resulting in energy waste as well as gaps in TCES research. From an exergy perspective, heat energy is usually considered as low-grade energy; in particular, it is difficult to recycle energy when the temperature of heat decreases.

*Corresponding author. Email-address: kubota.mitsuhiro@material.nagoya-u.ac.jp

Transition metal oxides are considered as promising candidates for TCES systems. Because of its multivalent property and abundance of ore resources, Mn provides a series of promising redox reactions and economic feasibility. Manganese oxides exist in different phases (MnO_2, Mn_2O_3, Mn_3O_4, and MnO) from low to high temperature. Although the transition of MnO_2 and Mn_2O_3 occurred at low temperature (500 °C), it did not exhibit reversibility[5]. Lei et al.[6] proposed Mn_2O_3/MnO redox couple for TCES purposes, but the reversibility of MnO to Mn_3O_4 remains unclear. Moreover, the main drawback of the Mn_2O_3/ Mn_3O_4 redox couple is slow oxidation kinetics. On the other hand, iron oxides (Fe_2O_3/Fe_3O_4) have been less investigated among metal oxides, likely because of their high reduction temperature (1400 °C) which causes difficulty in reactor design and application[7,8]. However, ferrites have been widely studied by some research groups for thermochemical hydrogen production (thermochemical water splitting process)[9,10,11].

Recently, manganese-iron binary oxide systems have attracted lots of attention in the field of TCES, because their improved kinetics performance and moderate reaction temperature. Carrillo et al.[12] studied the redox kinetics of $(Mn_{0.8}Fe_{0.2})_2O_3$, Al-Shankiti et al.[13] and Hamidi et al.[14] investigated oxidation and reduction kinetics of $(Mn_{0.33}Fe_{0.67})_2O_3$ respectively. A lab-scale packed bed reactor of $(Mn_{0.75}Fe_{0.25})_2O_3$ was established by Wokon et al.[15], which also showed the possibility of Mn-Fe oxide system as a series of promising TCES materials.

However, neither single or binary manganese-iron oxides show the ability to work at medium-high temperatures, new component should be introduced into the system. In our previous research, we investigated $SrMO_{3-\delta}$ (M = Co, Fe, Mn) perovskites as heat storage media and summarized the requirements of medium-high temperature TCES[16]. Whereas the redox reaction of perovskite is not accompanied by noticeable phase change, resulting in a small heat storage capacity even though they are able to react at relatively lower temperatures. Therefore, more promising candidates for medium-high temperature TCES are required.

In 2009, Kato et al.[17] investigated the oxygen storage capacity of delafossite $CuMO_2$ (M = Al, Fe, Mn, Ga). They claimed that the oxygen storage capacity values of $CuMnO_2$ and $CuFeO_2$ were quite larger than those of $CuAlO_2$, $CuGaO_2$ and CeO_2-based materials, and their oxygen storage behavior can occur at low temperatures (300-600 °C). Later, Kato's research group explored Cu-based rare earth element delafossite $CuLaO_2$ and $CuYO_2$ as new oxygen storage materials[18] with oxygen storage capacity far better than those of conventional CeO_2-related materials, used as promoters of automobile catalysts. Recently, Huang et al.[19] reported enhanced oxygen diffusion and storage capacity of monoclinic crednerite $CuMnO_2$ at a lower temperature by surface modification with CeO_2.

Based on previous research, Cu-based delafossite material showed unique property to re-oxidize at a relatively low temperature, satisfying the requirement of medium-high temperature TCES. Furthermore, the obvious phase change may possess a larger reaction enthalpy, that is, a larger heat storage capacity than Sr-based perovskites. However, the targets of oxygen storage and heat storage

research are different; the former focuses more on the oxidation process, while the latter focus on the reversibility of the reaction, heat storage capacity, and durability. In addition, more specific results are required to demonstrate the feasibility of Cu-based spinel/delafossite couples for medium-high temperature TCES.

Herein, Cu-based spinel/delafossite couples with Mn and Fe as a second cation were synthesized using a modified Pechini method to explore medium-high temperature (500-1000°C) TCES material. Physicochemical properties were investigated using XRD and SEM. Redox behavior and cyclability were studied using TGA, phase diagrams and SEM. Oxidation enthalpy of each delafossite sample was measured using DSC.

2. Experimental approach

2.1 Synthesis

Oxidation state CuM_2O_4 (M=Mn, Fe) spinel and reduction state $CuMO_2$ (M=Mn, Fe) delafossite were synthesized by a modified Pechini method[20]. Stoichiometric metal nitrate salts (1:1) were dissolved in deionized water, and citric acid was added to the solution at a ratio of 1:2 (metal cation: CA). Ethylene glycol was added as a reactant for polyesterification, the pH of solution was adjusted to 9 using an ammonia solution. The solution was stirred at 120 °C for 4 h, then dried in vacuum oven for 24 h. The obtained gel was pre-calcined at 500 °C for 1 h, after grinding, the powder was heated at 960-1000 °C for 12 h in different gas atmospheres subsequently. The specific synthesis conditions are listed in Table 1. For convenience, the samples heated in an oxidizing atmosphere are denoted as O-CuM (M = Mn, Fe), and the samples heated in a reducing atmosphere are denoted as R-CuM.

Table 1. Synthesis condition of each sample

M	Temperature (°C)	Atmosphere	Abb.
Mn	960	Air	O-CuMn
Mn	960	Ar	R-CuMn
Fe	1000	Air	O-CuFe
Fe	1000	Ar	R-CuFe

2.2 Structural characterization

Structure of the pre-calcined, O-CuM, and R-CuM samples were investigated using X-ray Diffraction (XRD) (SmartLab, Rigaku Corp.). Crystalline phase of each sample was analyzed using PDXL2 (Rigaku Data Analysis Software).

2.3 Morphological investigation

Particle morphologies of the as-prepared O-CuM and R-CuM were observed by Scanning Electron Microscopy (SEM) (JSM-7500F, JEOL Ltd.).

2.4 Redox test

Redox capacity of oxidation state sample was investigated by Thermogravimetric Analysis (TGA) (STA7300, HITACHI High-Tech Science Corp.). Two different programs were performed. First one consisted of heating and cooling step from 500 °C to 1000 °C ~ 1065 °C at a rate of 20 °C/min in synthetic air flow. The second temperature program was similar to the first one but heated to 900 °C ~ 950 °C in N_2 flow, then re-oxidized at 600 °C ~ 650 °C in air, aiming to investigate the reduction depth and medium temperature re-oxidization ability of each sample.

2.5 Oxidation enthalpy measurement

The reduction state (R-CuM) samples were chosen for oxidation enthalpy measurements using Differential Scanning Calorimetry apparatus (DSC) (DSC-60, Shimadzu Corp.). Isothermal oxidation method was adopted in this study. After heating to an appropriate temperature under N_2 protection, the gas was shifted to synthetic air when temperature was stable. The significant exothermic peak was monitored by DSC, then analyzed by TA-60WS software (Shimadzu Corp.).

2.6 Cyclability test

A 20 cycles program was set up for cyclability test, consisting of continuous heating and cooling step from 500 °C to 1000 °C in synthetic air; however, the holding time of each cycle was shortened to 10 mins. The SEM morphology of 10 cycles and 20 cycles samples were studied to verify their durability. To further elucidate the redox mechanism of samples, XRD crystallite size analysis of the as-prepared sample and 20 cycles sample were performed.

3. Results and discussion

3.1 Physicochemical characterization of materials

The pre-calcined and as-prepared samples were characterized using XRD to determine preparation mechanism and crystal structure, the summary results are listed in Table 2.

Table 2. Main phase, crystal structure and PDF-code of each sample

Sample	Main phase	Crystal Structure	PDF-#
Pre-CuMn	$Cu_{1.5}Mn_{1.5}O_4$	Cubic, F (0)	00-035-1172
	CuO	Monoclinic, Cc (9)	01-080-1916
O-CuMn	$CuMn_2O_4$	Cubic, Fd-3m (227)	01-074-1919
	CuO	Monoclinic, C2/c (15)	01-080-1268
R-CuMn	$CuMnO_2$	Monoclinic, C2/m (12)	00-050-0860
	$Cu(Cu_{0.04}Mn_{0.96})O_2$	Monoclinic, C2/m (12)	01-083-0034

Pre-CuFe	$Cu_{0.75}Fe_{2.25}O_4$	Cubic, Fd-3m (227)	01-073-2316
	CuO	Monoclinic, Cc (9)	01-080-1916
O-CuFe	$CuFe_2O_4$	Tetragonal, I41/amd (141)	01-072-1174
	CuO	Monoclinic, C2/c (15)	01-080-1268
R-CuFe	$CuFeO_2$	Trigonal, R-3m (166)	01-070-6670

Pechini method has been used for synthesizing lots of mixed metal oxides because of its versatile and component controllability. Through this method, metallic cations are dispersed in the skeleton frame, which formed by the polyesterification of citric acid and ethylene glycol. Combined with the pre-calcination process, the organic skeleton frame was removed. As shown in Table 2, the main phase of pre-calcined sample reveals that simple CuO and unsaturated phase were generated initially. When temperature continued to increase, Cu-based spinel gradually formed. The detailed mechanism is similar to those reported in our previous research[16].

The typical XRD patterns of O-CuM and R-CuM are shown in Figure 1. From the XRD results, all Cu-based spinels did not exhibit a pure phase but showed a mixture of corresponding spinel and CuO, mainly because the amount of raw metal nitrates was equivalence. It is interesting to note that only R-CuFe showed pure $CuFeO_2$ phase (PDF-01-070-6670). However, R-CuMn exhibited two similar phases, $CuMnO_2$ (PDF-00-050-0860) and $Cu(Cu_{0.04}Mn_{0.96})O_2$ (PDF-01-083-0034). Huang et al.[19] claimed that during the heating process of spinel $Cu_yMn_{3-y}O_4$ under air, the spinel could be easily converted to $Cu_{1+y'}Mn_{1-y'}O_2$ rather than $CuMnO_2$ [Eq. (2)],

$$\frac{1}{3-y}Cu_yMn_{3-y}O_4 + \frac{3-2y}{3-y}CuO \Leftrightarrow$$

$$\alpha Cu_{x'}Mn_{3-x'}O_4 + \frac{2-\alpha}{2}Cu_{1+y'}Mn_{1-y'}O_2 + \frac{1}{6-2y} - \frac{\alpha}{2}O_2 \quad (2)$$

where $\alpha = 2y'/(3+3y'-2x')$.

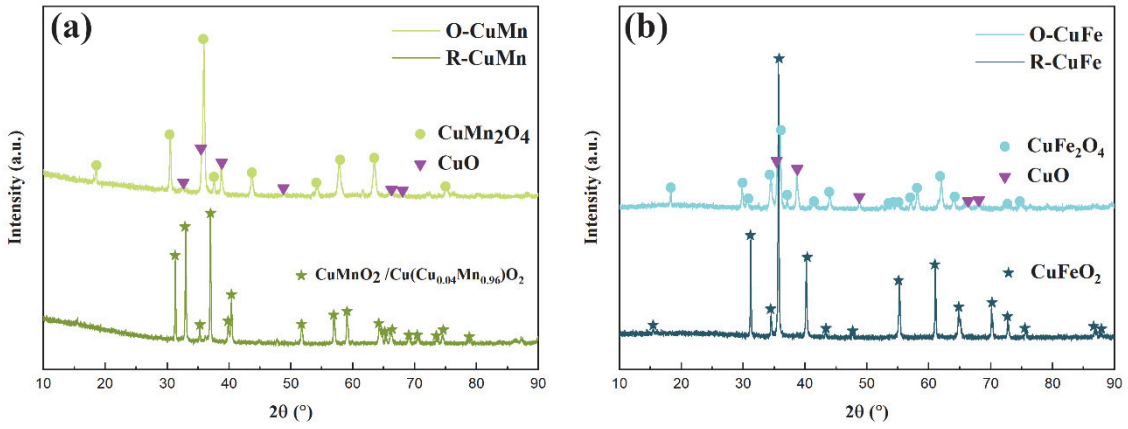

Figure 1. XRD patterns of (a) O-CuM; (b) R-CuM

The SEM images of as-prepared O-CuMn and R-CuMn are shown in Figure 2, while as-prepared O-CuFe and R-CuFe are shown in Figure 3. The low magnification image of O-CuMn (Figure 2a) reveals that the particles agglomerated to generate large blocks, and some small debris can be observed because of grinding before SEM observation. However, R-CuMn (Figure 2c) exhibited well-distributed particles with a size of 2~3 μm. It should be noted that the particles of O-CuMn could also be considered as irregular strips as same as O-CuFe, which presented in Figure 3a, but aggregated. A prominent terrace-like structure can be seen in the high magnification image of O-CuMn and R-CuMn (Figure 2b, Figure 2d). Kato et al.[17] and Huang et al.[19] described the delafossite-type oxides such as $CuFeO_2$, $CuMnO_2$, $CuLaO_2$ and $CuYO_2$ which have a layered structure consisting of edge-shared MO_6 octahedra, and two coordinated Cu^+ cations at the interlayer sites. However, they did not perform any morphological investigation of delafossite-type materials. On the other hand, it is easy to deduce that O-CuMn ($CuMn_2O_4$) also has the same layered structure and is regular enough to be seen. Interestingly, R-CuFe showed flaky structure with holes at low magnification (Figure 3c). However, the terrace-like structure, namely the edge-shared MO_6 octahedra layers can be recognized barely even in high magnification view of O-CuFe and R-CuFe (Figure 3b, Figure 3d), and the length of layers were less than 1 μm.

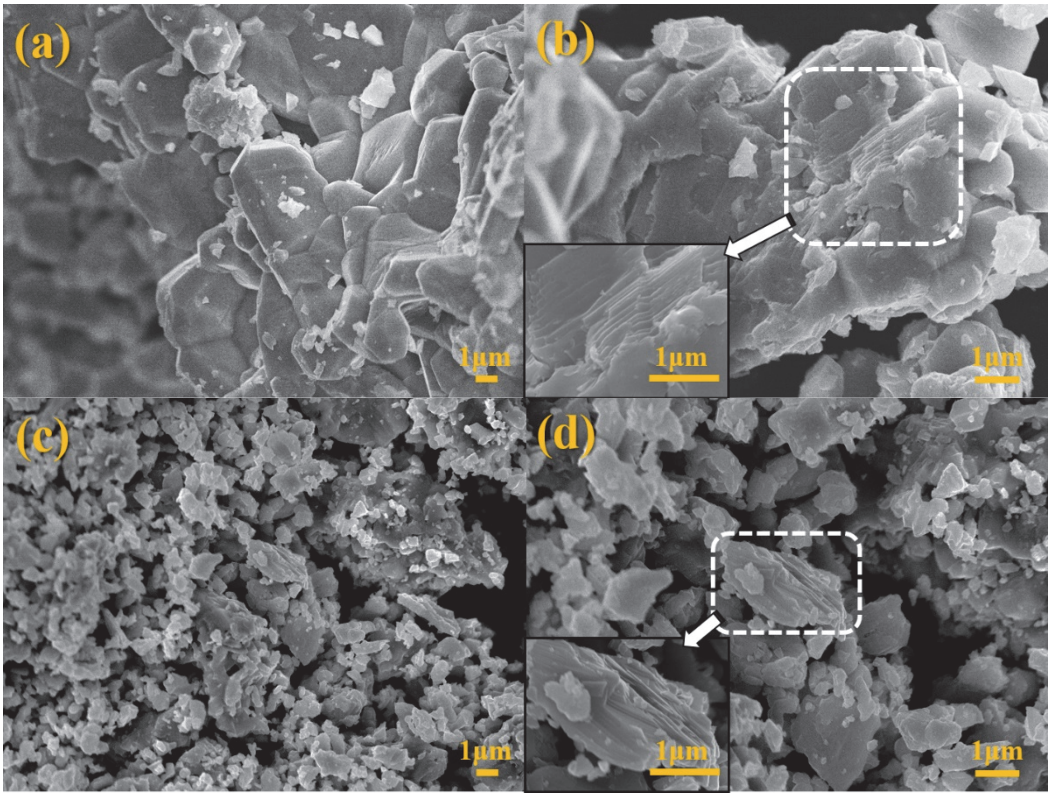

Figure 2. SEM images of as-prepared samples: (a-b) for O-CuMn; (c-d) for R-CuMn

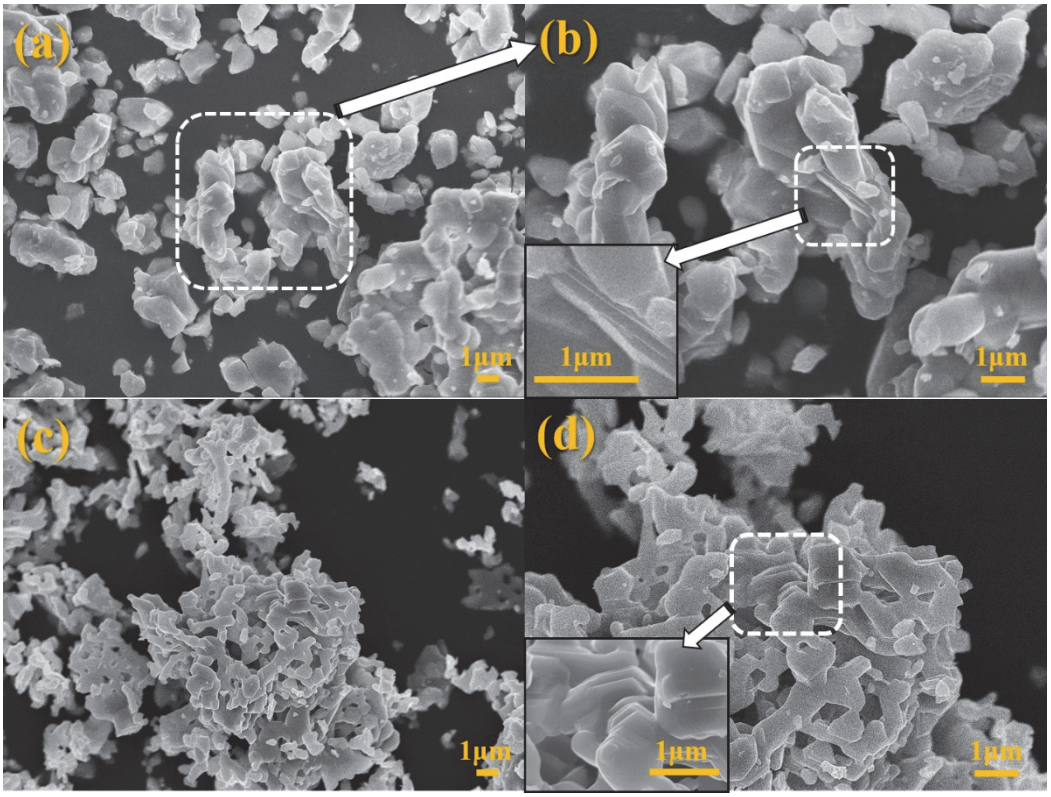

Figure 3. SEM images of as-prepared samples: (a-b) for O-CuFe; (c-d) for R-CuFe

3.2 Redox capacity

The redox behavior of O-CuMn is shown in the Figure 4a, O-CuMn exhibited approximately 4% change in mass when heated up to 1000 °C. In the second cycle, the mass changed rapidly at 980 °C ($T_{onset\text{-}red}$), which is different from the smooth behavior presented in the first cycle. During oxidation process, the reaction occurred at 900 °C ($T_{onset\text{-}oxi}$) with an intense DTA signal peak. However, the significant endothermic peak cannot be detected in neither one of them during reduction. Compared with the Cu-Mn-O phase diagram which shown in Figure 4b, spinel + CuO mixed phase was observed when x(Cu) = 0.5 at the temperature below 900 °C. This conclusion consistent with the XRD results obtained in Figure 1a that a small amount of CuO was existing. When temperature keeps raising, it will convert to spinel + delafossite mixed phase, corresponding to 4% change in mass shown in Figure 4a. However, the spinel peaks were not detectable from the XRD pattern of R-CuMn, which may be related to its small amount. Driessens et al.[21] summarized delafossite ($Cu_yMn_{1-y}O$, $0.54<y<0.6$, hexagonal) and crednerite ($Cu_yMn_{1-y}O$, $0.5<y<0.53$, monoclinic) into two different phases. From phase diagram of Cu-Mn-O, the crednerite can be considered as the deeper reduced phase than delafossite. However, it is very difficult to convert the spinel structure $CuMn_2O_4$ to the pure crednerite structure $CuMnO_2$ in normal air atmosphere at the temperature below 1000 °C.

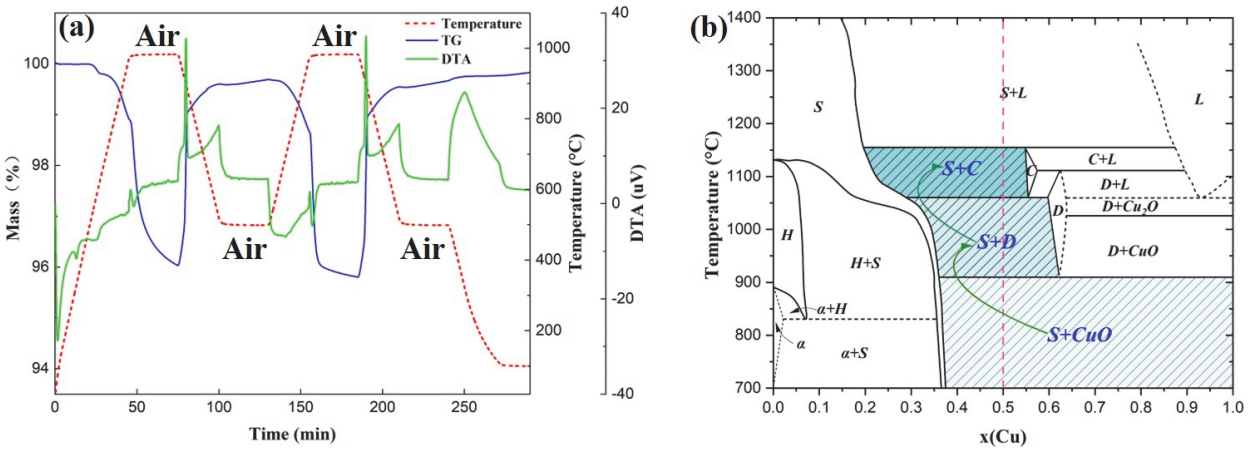

Figure 4. O-CuMn: (a) redox in air from 500 °C to 1000 °C; (b) Cu-Mn-O phase diagram (pO_2 = 0.21 atm), replotted from previous literature[21] (H = hausmannite, S = spinel, C = crednerite, D = delafossite, α = α-Mn_2O_3)

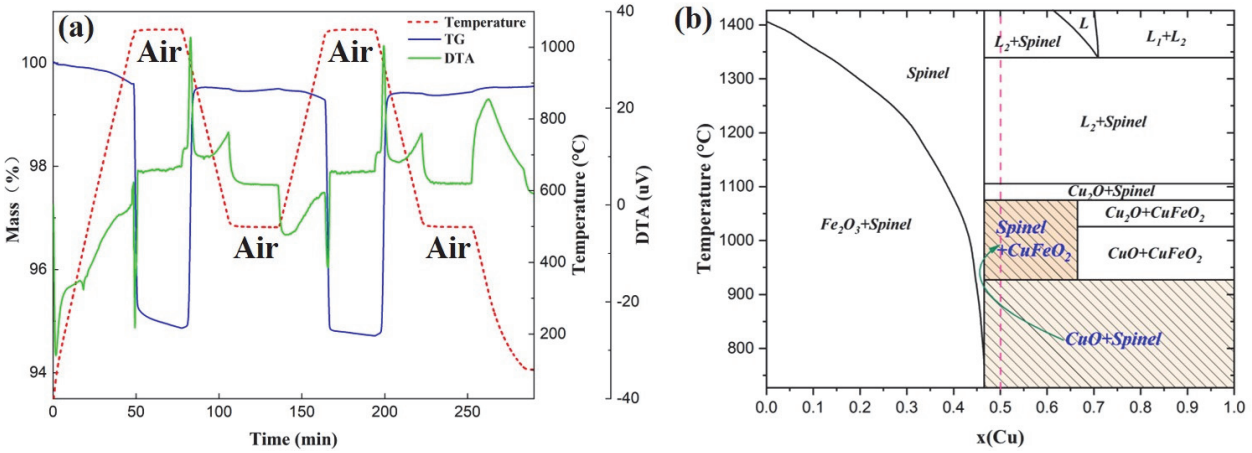

Figure 5. O-CuFe: (a) redox in air from 500 °C to 1065 °C; (b) Cu-Fe-O phase diagram (pO_2 = 0.21 atm), replotted from Khvan et al.[22]

The redox behavior of O-CuFe (Figure 5a) was similar to that of O-CuMn, but required a higher temperature for reduction (1030 °C) and oxidation (950 °C), showing a 5 % change in mass. In contrast to O-CuMn, the endothermic peak of O-CuFe accompanied by reduction reaction was obvious enough. From Cu-Fe-O phase diagram (Figure 5b) replotted from the research of Khvan et al.[22], CuO + spinel mixed phase convert to spinel + $CuFeO_2$ mixed phase at the temperature of 925 °C. Similar to R-CuMn mentioned above, the spinel peaks were also not shown in the XRD pattern of R-CuFe due to its small amount. However, according to the earlier literature, this conversion occurs at 1004 °C[23] and 1015 °C[24], which are very close to our result.

In our pre-experiment, in order to explore the re-oxidation ability of each sample under medium temperature range, O-CuM was reduced in N_2 flow, then undergoes isothermal oxidation in the

temperature of 400-700 °C. After comparing their conversion rate and re-oxidation reaction time, a typical figure was shown in Figure 6. As shown in Figure 6a, a deeper reduction of O-CuMn occurred with about 6% change in mass at lower 850 °C. Furthermore, through the isothermal oxidation at 600 °C, only a mild exothermic peak was detected, suggesting that a lower temperature can control the heat release rate. While O-CuFe exhibited almost same reduction depth while reduced in N_2, indicating that there was only a type of phase transition occurred (Figure 6b).

From Figure 4a and Figure 5a, O-CuMn and O-CuFe showed hysteresis (80 °C for both) between reduction onset temperature and oxidation onset temperature similar to other famous redox couples, for example, $T_{hysteresis}$ of 30 °C for Co_3O_4/CoO and $T_{hysteresis}$ of 200 °C for Mn_2O_3/Mn_3O_4[25]. However, according to Figure 6, the reduced O-CuMn and O-CuFe also showed the ability to re-oxidize at the temperature much lower than oxidation onset temperature. This phenomenon can be explained by activation energy comparison of oxidation, but from the perspective of structure analysis, the existence of MO_6 octahedra may also promote this behavior. According to the structural analysis of another well-known metal oxide, perovskite (the general chemical formula is ABO_3), it also consists of MO_6 octahedra. Specifically, the lattice oxygen of perovskite is released in a nonstoichiometric way during heating, resulting in $ABO_{3-\delta}$ continuous phase. Zhang et al.[26] assessed Ba- and Sr-based perovskites for solar energy storage, $SrCoO_3$, $SrFeO_3$, and $BaCoO_3$ showed ability to reduce in the range of 500 °C-1000 °C, then re-oxidized at 600 °C. Jeen et al.[27] reported that they lowered the redox temperature (200-300 °C) of $SrCoO_{3-\delta}$ by epitaxial stabilization, and the phase change between perovskite $SrCoO_{3-\delta}$ and brownmillerite $SrCoO_{2.5}$ can switch in a considerably short time (<1 min). It should be mentioned that even possess the similar structure, perovskite exhibits point-shared MO_6 octahedra while spinel/delafossite are edge-shared structure.

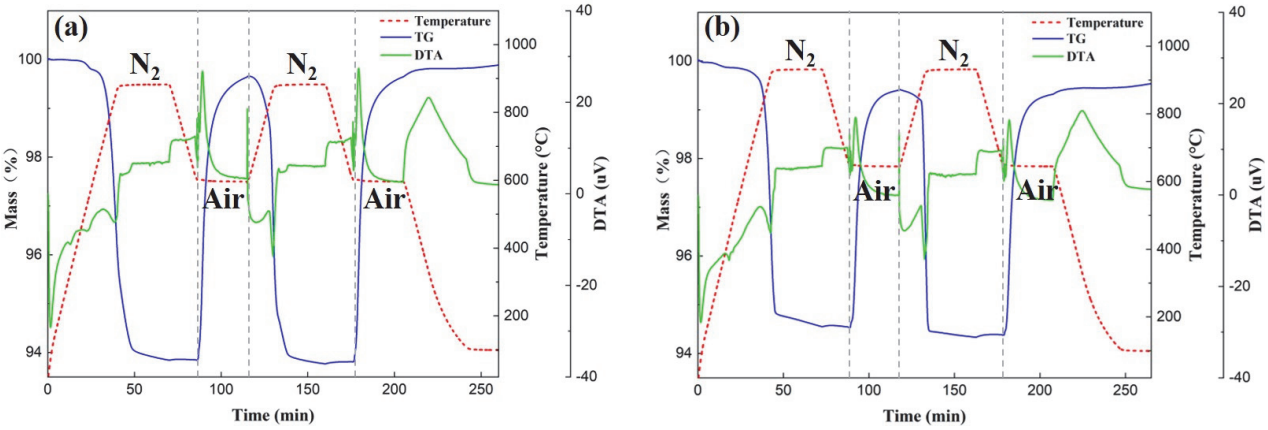

Figure 6. (a) O-CuMn: heated to 900 °C in N_2, then re-oxidized at 600 °C in air; (b) O-CuFe: heated to 950 °C, then re-oxidized at 650 °C in air

3.3 Oxidation enthalpy measurement

R-CuMn and R-CuFe were chosen for oxidation enthalpy measurements. The so-called isothermal oxidation method is that the sample was heated to an appropriate temperature in the N_2 flow protection,

then the gas was shifted to air when the temperature and DSC signal were stable. A significant exothermic peak was detected by the DSC apparatus. The oxidation enthalpy of R-CuMn and R-CuFe were 258.32 ± 15.31 kJ/kg (1402.68 ± 83.13 kJ/L) and 190.35 ± 4.81 kJ/kg (1048.83 ± 26.50 kJ/L), respectively. It should be noted that the oxidation enthalpy of $CuMnO_2$ we report here is quite larger than previous literature (145 kJ/kg)[28,29], mainly because the R-CuMn is the deeper and purer reduction state than those samples reduced via TG in several hours. On the other hand, the oxidation enthalpies of Cu-based redox couples were several times larger than that of Sr-based perovskites (81.7 ± 3.4 kJ/kg-ABO3 (473.5 ± 20.0 kJ/L)) we reported in previous research[16].

A smooth baseline can be distinguished from Figure 7a, indicating the specific heat capacity of reactant and product were almost equivalent. However, R-CuFe showed a rugged baseline (Figure 7b) making it difficult to calculate more precise values.

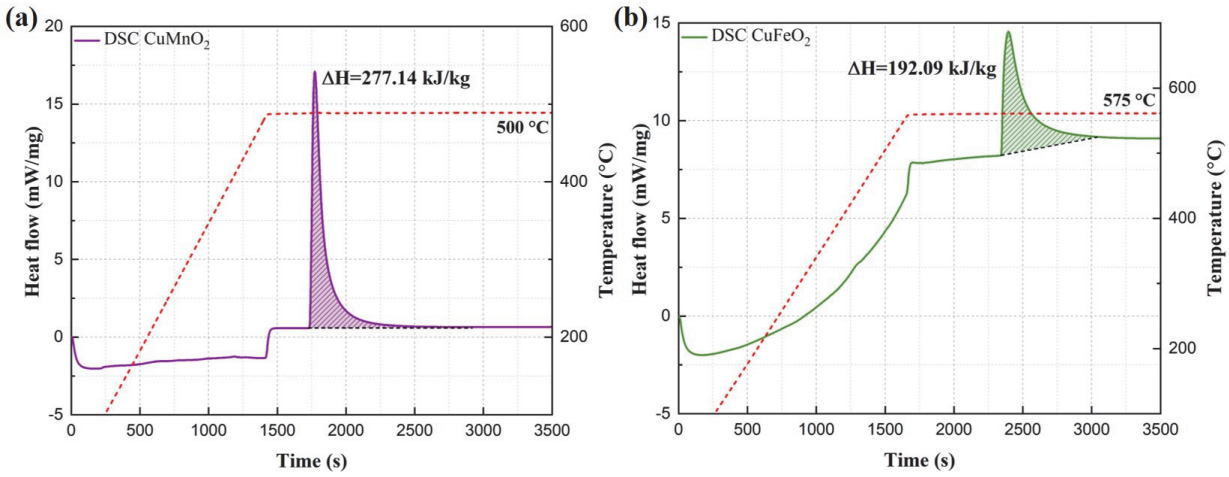

Figure 7. DSC curve of (a) R-CuMn and (b) R-CuFe with isothermal oxidation method

3.4 Cyclability test

Owing to its favorable redox behavior in the range of 500-1000 °C and relatively larger oxidation enthalpy, O-CuMn was chosen for further cyclability study. A 20 cycles program was set up for cyclability test, as shown in the Figure 8a. In the first cycle, O-CuMn did not show an ideal reduction depth, which only reached 3.2% change in mass. However, it is interesting to note that as the number of cycles increases, the depth of reduction also gradually enhanced. After 13 cycles, the change in mass was stable at 4% approximately. This suggests that O-CuMn undergoes run-in period to reach favorable redox behavior in shorten 10 minutes holding time at high temperature. Compared with the as-prepared O-CuMn shown in Figure 2b, 10 cycles and 20 cycles (Figure 8b-c) exhibited a phenomenon that the terrace-like structure melted. To investigate the redox mechanism better, the crystallite size analysis was performed. The crystallite size was calculated using the data extracted from XRD (Figure 9), the as-prepared sample showed a crystallite size of 27 nm and 20 cycles sample showed a larger size of 34 nm. It should be noted that the XRD pattern of 20 cycles O-CuMn

slightly shifted to low angle (<1°), indicating the interplanar spacing increased based on Bragg's law equation. The small crystallite size and interplanar spacing may pose difficulty for lattice oxygen to be released from a tight crystal structure in a short time, thus exhibiting a macroscopically smaller oxygen exchange capacity. After 20 cycles, the crystals continue to grow and formed larger crystalline sizes, the ordered crystal structure may guide oxygen atoms to find binding sites more quickly, accelerating the oxygen exchange rate in a short time.

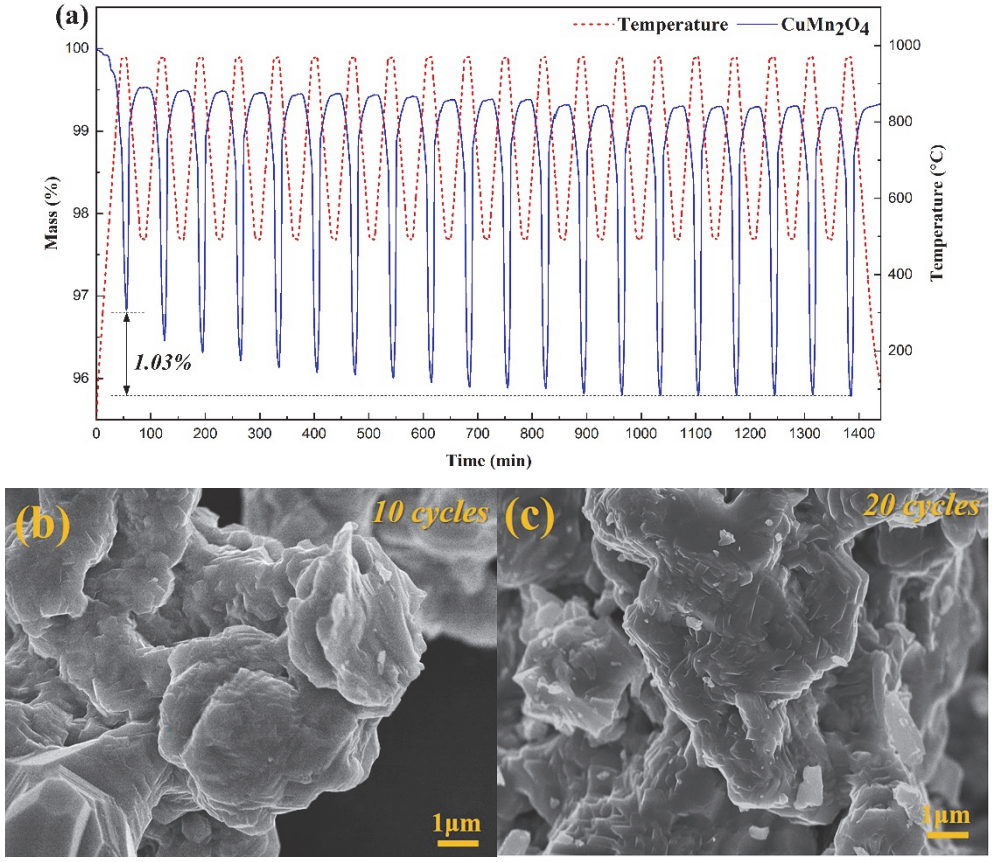

Figure 8. (a) Cyclability test of O-CuMn under synthetic air; (b) SEM image of the 10 cycles $CuMn_2O_4$; (c) SEM image of the 20 cycles $CuMn_2O_4$

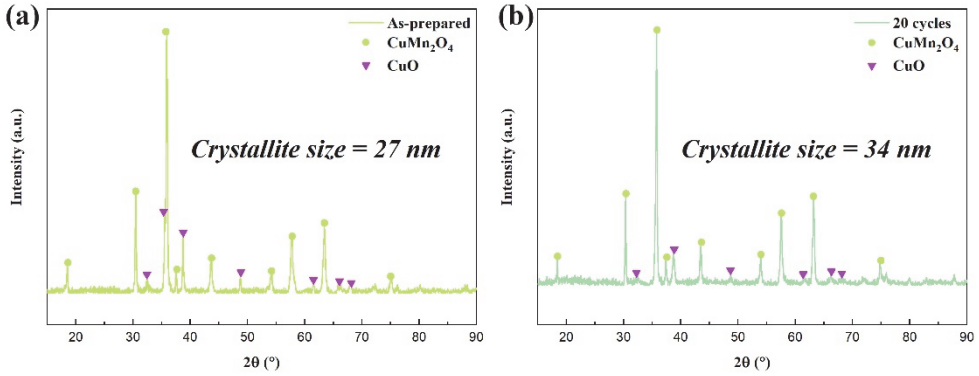

Figure 9. (a)(b) XRD patterns of as-prepared and 20 cycles O-CuMn

4. Conclusions

At present, redox-type TCES technology is still in the early stage of development, and the most researchers focus on the utilization of solar heat in high temperature range. Moreover, due to the inherent high onset temperature of metal oxides, the research in the field of medium-high temperature field is almost at a blank stage. In this study, we investigated Cu-based spinel/delafossite couples with Mn and Fe as a second cation, and explored the feasibility of redox-type TCES system in medium-high temperature range. Pechini method was chosen for preparation of all samples because its high component controllability. The physicochemical properties of samples were characterized using XRD and SEM morphology. From the XRD results, O-CuMn and O-CuFe only showed CuM_2O_4 + CuO mixed phase, suggesting that the input ratio of raw materials influences the phase significantly. It is worth to noting that R-CuFe exhibited a pure $CuFeO_2$ delafossite phase, which corresponds well to the phase diagram of Cu-Fe-O. However, R-CuMn exhibited a mixed phase of $CuMnO_2$ and $Cu(Cu_{0.04}Mn_{0.96})O_2$, and it is difficult to determine their respective proportions. According to the SEM investigation of O-CuM and R-CuM, terrace-like structure can be distinguished, it may relate to the existence of edge-shared MO_6 octahedra layered structure. O-CuMn showed favorable redox behavior in the range of 500~1000 °C, while O-CuFe possesses higher reduction onset temperature (1030 °C). The reduced O-CuMn and O-CuFe were able to re-oxidize at 600 °C and 650 °C under air atmosphere even though the temperatures were much lower than their oxidation onset temperature, and the existence of MO_6 octahedra structure may promote this phenomenon. R-CuMn and R-CuFe were chosen for heat storage capacity measurement via DSC apparatus, the oxidation enthalpies were 258.32 ± 15.31 kJ/kg (1402.68 ± 83.13 kJ/L) and 190.35 ± 4.81 kJ/kg (1048.83 ± 26.50 kJ/L), respectively. From further 20 cycles cyclability study of O-CuMn, the depth of reduction gradually enhanced and the melted terrace-like structure occurred as the number of cycles increases. After run-in period of 13 cycles, the change in mass was stable at approximately 4%.

Through this research, $CuMn_2O_4/CuMnO_2$ couple can be regarded as a promising candidate, however, the problem of relatively high reduction temperature, the specific relationship between the crystal structure and reaction temperature, and undefined kinetics require further investigation in the future.

Acknowledgement

This research was supported by "Knowledge Hub Aichi", Priority Research Project (3rd term) from Aichi Prefectural Government, Japan

Reference

(1) Carrillo, A. J.; González-Aguilar, J.; Romero, M.; Coronado, J. M. Solar Energy on Demand: A Review on High Temperature Thermochemical Heat Storage Systems and Materials. *Chem. Rev.* **2019**, *119* (7), 4777–4816.

(2) Wu, S.; Zhou, C.; Doroodchi, E.; Nellore, R.; Moghtaderi, B. A Review on High-Temperature Thermochemical Energy Storage Based on Metal Oxides Redox Cycle. *Energy Convers. Manag.* **2018**, *168* (April), 421–453.

(3) Babiniec, S. M.; Coker, E. N.; Miller, J. E.; Ambrosini, A. Investigation of LaxSr1-XCoyM1-YO3-δ (M=Mn, Fe) Perovskite Materials as Thermochemical Energy Storage Media. *Sol. Energy* **2015**, *118*, 451–459.

(4) Babiniec, S. M.; Coker, E. N.; Miller, J. E.; Ambrosini, A. Doped Calcium Manganites for Advanced High-Temperature Thermochemical Energy Storage. *Int. J. Energy Res.* **2016**, *40* (2), 280–284.

(5) Zaki, M. I.; Hasan, M. A.; Pasupulety, L.; Kumari, K. Thermochemistry of Manganese Oxides in Reactive Gas Atmospheres: Probing Catalytic MnOx Compositions in the Atmosphere of CO+O2. *Thermochim. Acta* **1998**, *311* (1–2), 97–103.

(6) Lei, Q.; Bader, R.; Kreider, P.; Lovegrove, K.; Lipiński, W. Thermodynamic Analysis of a Combined-Cycle Solar Thermal Power Plant with Manganese Oxide-Based Thermochemical Energy Storage. *E3S Web Conf.* **2017**, *22, id.00102*.

(7) Block, T.; Schmücker, M. Metal Oxides for Thermochemical Energy Storage: A Comparison of Several Metal Oxide Systems. *Sol. Energy* **2016**, *126*, 195–207.

(8) Agrafiotis, C.; Block, T.; Senholdt, M.; Tescari, S.; Roeb, M.; Sattler, C. Exploitation of Thermochemical Cycles Based on Solid Oxide Redox Systems for Thermochemical Storage of Solar Heat. Part 6: Testing of Mn-Based Combined Oxides and Porous Structures. *Sol. Energy* **2017**, *149*, 227–244.

(9) Scheffe, J. R.; Li, J.; Weimer, A. W. A Spinel Ferrite/Hercynite Water-Splitting Redox Cycle. *Int. J. Hydrogen Energy* **2010**, *35* (8), 3333–3340.

(10) Scheffe, J. R.; McDaniel, A. H.; Allendorf, M. D.; Weimer, A. W. Kinetics and Mechanism of Solar-Thermochemical H2 Production by Oxidation of a Cobalt Ferrite-Zirconia Composite. *Energy Environ. Sci.* **2013**, *6* (3), 963–973.

(11) Fresno, F.; Yoshida, T.; Gokon, N.; Fernández-Saavedra, R.; Kodama, T. Comparative Study of

the Activity of Nickel Ferrites for Solar Hydrogen Production by Two-Step Thermochemical Cycles. *Int. J. Hydrogen Energy* **2010**, *35* (16), 8503–8510.

(12) Carrillo, A. J.; Serrano, D. P.; Pizarro, P.; Coronado, J. M. Understanding Redox Kinetics of Iron-Doped Manganese Oxides for High Temperature Thermochemical Energy Storage. *J. Phys. Chem. C* **2016**, *120* (49), 27800–27812.

(13) Al-Shankiti, I. A.; Ehrhart, B. D.; Ward, B. J.; Bayon, A.; Wallace, M. A.; Bader, R.; Kreider, P.; Weimer, A. W. Particle Design and Oxidation Kinetics of Iron-Manganese Oxide Redox Materials for Thermochemical Energy Storage. *Sol. Energy* **2019**, *183* (March), 17–29.

(14) Hamidi, M.; Bayon, A.; Wheeler, V. M.; Kreider, P.; Wallace, M. A.; Tsuzuki, T.; Catchpole, K.; Weimer, A. W. Reduction Kinetics for Large Spherical 2:1 Iron–Manganese Oxide Redox Materials for Thermochemical Energy Storage. *Chem. Eng. Sci.* **2019**, *201*, 74–81.

(15) Wokon, M.; Kohzer, A.; Linder, M. Investigations on Thermochemical Energy Storage Based on Technical Grade Manganese-Iron Oxide in a Lab-Scale Packed Bed Reactor. *Sol. Energy* **2017**, *153*, 200–214.

(16) Chen, X.; Kubota, M.; Yamashita, S.; Kita, H. Investigation of Sr-Based Perovskites for Redox-Type Thermochemical Energy Storage Media at Medium-High Temperature. *J. Energy Storage* **2021**, *38* (November 2020), 102501.

(17) Kato, S.; Fujimaki, R.; Ogasawara, M.; Wakabayashi, T.; Nakahara, Y.; Nakata, S. Oxygen Storage Capacity of CuMO2 (M = Al, Fe, Mn, Ga) with a Delafossite-Type Structure. *Appl. Catal. B Environ.* **2009**, *89* (1–2), 183–188.

(18) Kato, S.; Sato, H.; Ogasawara, M.; Wakabayashi, T.; Nakahara, Y.; Nakata, S. Oxygen Storage Capacity of Delafossite-Type CuLnO 2 (Ln = La, Y) and Their Stability under Oxidative/Reductive Atomosphere. *Solid State Sci.* **2012**, *14* (1), 177–181.

(19) Huang, X.; Ni, C.; Zhao, G.; Irvine, J. T. S. Oxygen Storage Capacity and Thermal Stability of the CuMnO2-CeO2 Composite System. *J. Mater. Chem. A* **2015**, *3* (24), 12958–12964.

(20) Pechini, M. P. Method of Pre Parng Lead and Alkalne Earth Titanates and Nobates and Coat. *US Pat. 3,330,697* **1967**, 2.

(21) Driessens, F. C. M. Phase Equilibria in the System Cu-Mn-O. *J. Inorg. Gen. Chem.* **1967**, *351* (1–2), 48–62.

(22) Khvan, A. V.; Fabrichnaya, O. B.; Savinykh, G.; Adam, R.; Seifert, H. J. Thermodynamic Assessment of the Cu-Fe-O System. *J. Phase Equilibria Diffus.* **2011**, *32* (6), 498–511.

(23) Schaefer, S. C.; Hundley, G. L.; Block, F. E.; McCune, R. A.; Mrazek, R. V. Phase Equilibria and X-Ray Diffraction Investigation of the System Cu-Fe-O. *Metall. Trans.* **1970**, *1* (9), 2557–2563.

(24) Jacob, K. T.; Fitzner, K.; Alcock, C. B. Activities in the Spinel Solid Solution, Phase Equilibria and Thermodynamic Properties of Ternary Phases in the System Cu-Fe-0. *Metall. Trans. B* **1977**, *8* (2), 451–460.

(25) Dizaji, H. B.; Hosseini, H. A Review of Material Screening in Pure and Mixed-Metal Oxide Thermochemical Energy Storage (TCES) Systems for Concentrated Solar Power (CSP) Applications. *Renew. Sustain. Energy Rev.* **2018**, *98* (May), 9–26.

(26) Zhang, Z.; Andre, L.; Abanades, S. Experimental Assessment of Oxygen Exchange Capacity and Thermochemical Redox Cycle Behavior of Ba and Sr Series Perovskites for Solar Energy Storage. *Sol. Energy* **2016**, *134*, 494–502.

(27) Jeen, H.; Choi, W. S.; Biegalski, M. D.; Folkman, C. M.; Tung, I. C.; Fong, D. D.; Freeland, J. W.; Shin, D.; Ohta, H.; Chisholm, M. F.; Lee, H. N. Reversible Redox Reactions in an Epitaxially Stabilized SrCoO x Oxygen Sponge. *Nat. Mater.* **2013**, *12* (11), 1057–1063.

(28) Hlongwa, N. W.; Sastre, D.; Iwuoha, E.; Carrillo, A. J.; Ikpo, C.; Serrano, D. P.; Pizarro, P.; Coronado, J. M. Exploring the Thermochemical Heat Storage Capacity of AMn2O4 (A = Li or Cu) Spinels. *Solid State Ionics* **2018**, *320*, 316–324.

(29) André, L.; Abanades, S.; Cassayre, L. Experimental Investigation of Co-Cu, Mn-Co, and Mn-Cu Redox Materials Applied to Solar Thermochemical Energy Storage. *ACS Appl. Energy Mater.* **2018**, *1* (7), 3385–3395.